Supporting Information

Contrast-enhanced sonography with biomimetic lung surfactant nanodrops

Alec N. Thomas[1,2], Kang-Ho Song[1], Awaneesh Upadhyay[1], Virginie Papadopoulou[3], David Ramirez[4], Richard K. P. Benninger[4], Matthew Lowerison[5,6], Pengfei Song[5,6], Todd W. Murray[1,7] and Mark A. Borden[1,7,*]

Affiliations: [1]Mechanical Engineering, University of Colorado, Boulder, USA. [2]Institute of Biomedical Engineering, Oxford University, Oxford, UK. [3]Joint Department of Biomedical Engineering, University of North Carolina at Chapel Hill & North Carolina State University, NC, USA. [4]Bioengineering, University of Colorado, Anschutz Medical campus, USA. [5]Electrical and Computer Engineering, University of Illinois, Urbana-Champaign, USA. [6]Beckman Institute for Advanced Science and Technology, University of Illinois, Urbana-Champaign, USA. [7]Biomedical Engineering, University of Colorado, Boulder, USA.

1. Viscoelastic Properties for a Microbubble Oscillating in the Linear Regime

A microbubble subjected to small perturbations can be modeled as a damped mass-spring system, where the compressible gas core and shell are analogous to a spring and the surrounding incompressible liquid is analogous to a mass. Following the analysis by Chatterjee and Sarkar[1], and later Marmottant et al.[2], the shell dilatational elasticity, χ, for microbubble driven in the linear regime is a function of the resonance frequency, f_0:

$$\chi = \pi^2 f_0^2 \rho R^3 - \frac{3}{4}\kappa P_0 R - \frac{(3\kappa - 1)\sigma}{2} \#(S1)$$

where ρ is the liquid density, R is the bubble radius, κ is the polytropic gas exponent, P_0 is the ambient pressure and σ is the interfacial tension (assumed zero for a non-dissolving microbubble[3,4]). The damping of the system is the sum of contributions from four sources: the re-radiation of sound from the bubble (ζ_r), the heat flow from the work to compress and expand the bubble (ζ_t), the friction from the surrounding fluid (ζ_v) and the shell viscosity (ζ_{shell}). The total damping ratio is:

$$\zeta = \zeta_r + \zeta_t + \zeta_v + \zeta_{shell} \#(S2)$$

From the experimentally determined resonance curve, the total damping ratio is computed by

$$\zeta = \frac{\Delta f}{f_0} \#(S3)$$

where Δf the full-width-half-maximum of the resonance curve, and ζ_{shell} is determined by subtracting the other damping terms, as described by Hoff[5]. The shell damping ratio is related to the interfacial surface viscosity κ_s by the following relation[6]:

$$\zeta_{shell} = \frac{\kappa_s}{\pi R^3 \rho f_0} \#(S4)$$

where it is seen that the surface viscosity is directly proportional to the shell damping ratio.

2. Size Distributions of Pre-Condensed Microbubbles

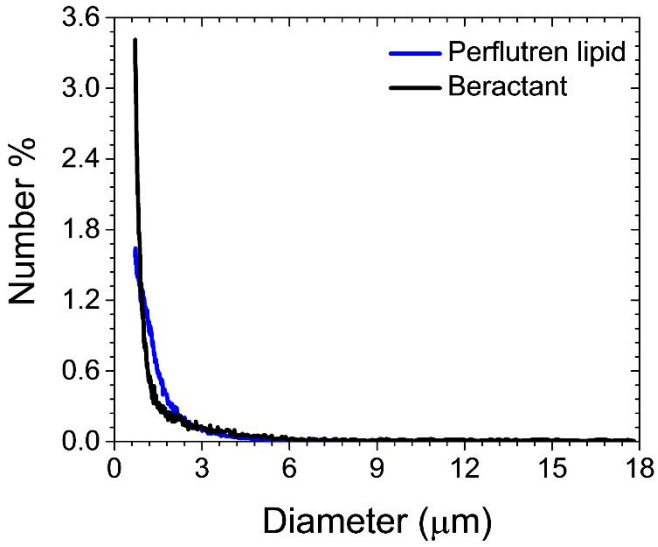

Supplementary Figure S1 | Number-weighted size distribution measured for Beractant (black) and Perflutren lipid (blue) after microbubbles were produced via mechanical agitation (n = 3), as measured with a Beckman Coulter Multisizer III. See Supplementary Table 1 for the average particle concentration, diameter, and span.

Supplementary Data Table S1 | Pre-condensed microbubble size distribution as determined with a Multisizer III.

Formulation	Concentration ± SD (per mL)	Mean Diameter ± SD (μm)	Diameter Span ± SD (μm)
Perflutren lipid	$3.41 \times 10^9 \pm 1.93 \times 10^8$	1.27 ± 0.03	1.13 ± 0.04
Beractant	$2.40 \times 10^9 \pm 5.82 \times 10^7$	1.32 ± 0.01	1.58 ± 0.04

3. Size Distributions of Beractant Microbubble-Condensed Nanodrops

Nanodrops were synthesized by condensation of Beractant microbubbles as described in the experimental section of the text. Size distribution of the resulting suspensions was determined by light scattering using the Malvern Zetasizer Nano ZS (Fig. S2), which is more sensitive to nanoparticles, and Beckman Coulter Multisizer III (Fig. S3), which measures larger particles. Samples were taken directly after nanodrop formation and then, to assess stability, after shipping from Colorado to Illinois, and then back to Colorado.

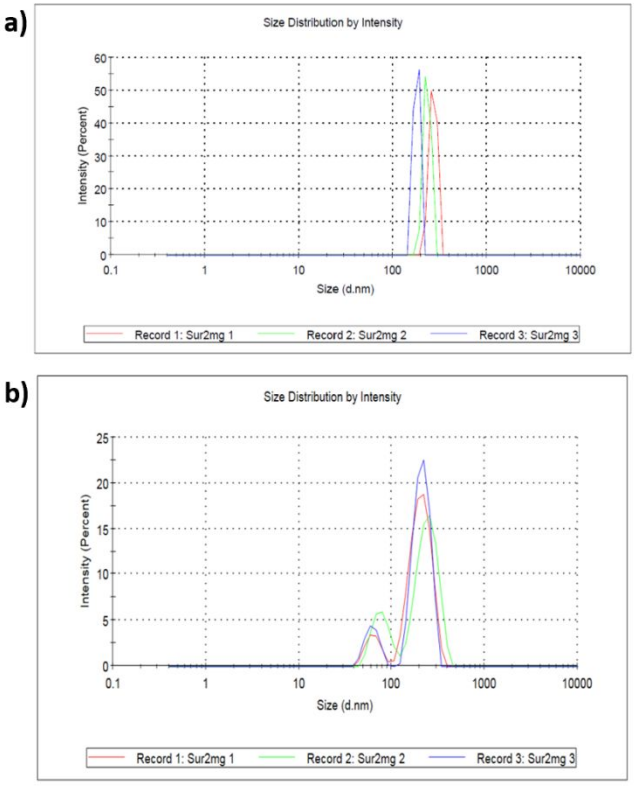

Supplementary Figure S2 | Intensity-weighted size distributions measured by the Zetasizer for three samples of Beractant nanodrops (a) just after microbubble condensation, and (b) after shipping from Colorado to Illinois and then back to Colorado. The peak of the distributions was between 200 and 300 nm diameter for both samples, although the older sample showed a wider distribution and a secondary peak at diameters below 100 nm.

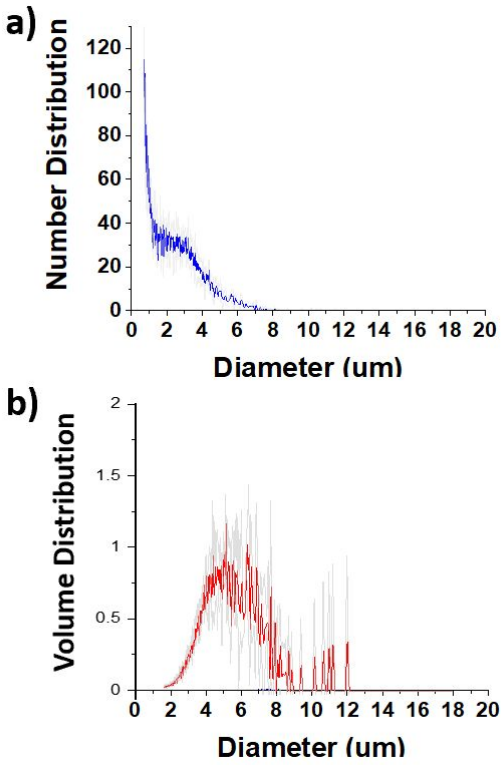

Supplementary Figure S3 | (a) Number- and (b) volume-weighted size distributions measured by the Multisizer for three samples of Beractant nanodrops just after microbubble condensation. Similar size distributions were obtained after shipping from Colorado to Illinois and then back to Colorado. Note the presence of particles between 1 and 10 μm diameter, especially when viewed in the volume-weighted mode.

4. *Echogenicity of Microbubbles Generated by ADV of Nanodrops*

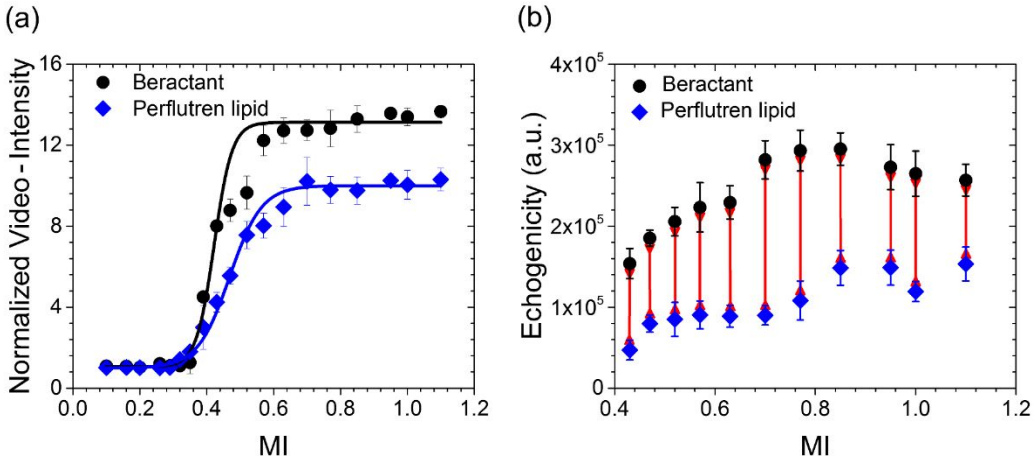

Supplementary Figure S4 | Echogenicity Characteristics during Acoustic Nanodrop Vaporization. (a) The maximum normalized echogenicity for each mechanical index (MI) tested with the clinical ultrasound machine using Beractant nanodrops or the Perflutren lipid nanodrops. The values were normalized to the background intensity at the lowest MI setting. The curves follow a similar trend displaying a maximum intensity at MI > 0.70 for both nanodrop types. (b) The measured echogenicity at each MI after 120 seconds of insonation. The red curve indicates the improvement in echogenicity between Beractant and Perflutren lipid.

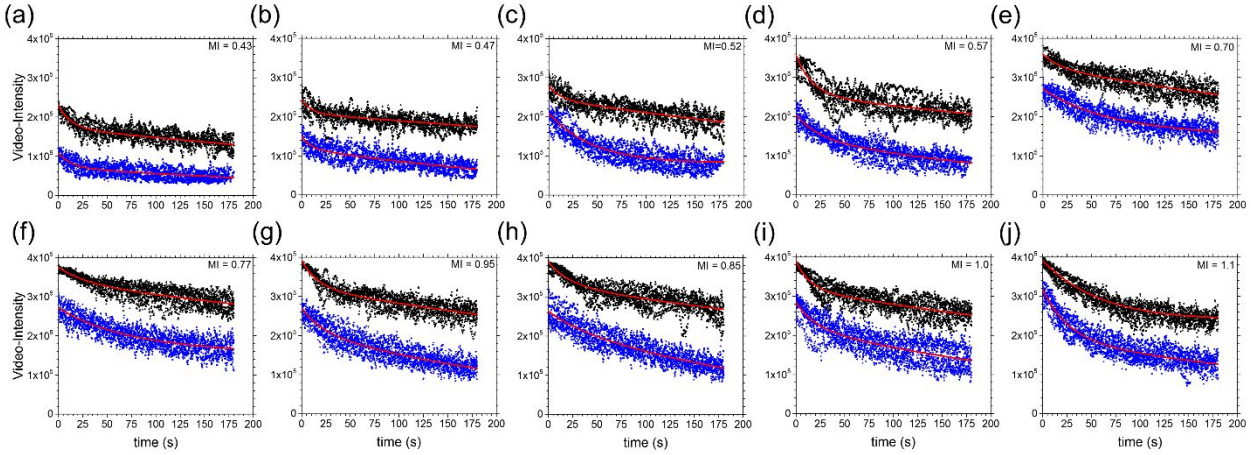

Supplementary Figure S5 | Increased echogenicity for Beractant vaporized nanodrops. The echogenicity data of vaporized Beractant nanodrops (black markers, n = 6) and Perflutren lipid nanodrops (blue markers, n = 6) at ten different mechanical indices using the clinical ultrasound scanner. The mechanical index (MI) is displayed in the upper right-hand corner of each plot. The red curve shows the best fit of a double exponential to the respective data.

5. References

(1) Chatterjee, D.; Sarkar, K. A Newtonian Rheological Model for the Interface of Microbubble Contrast Agents. *Ultrasound Med. Biol.* **2003**, *29* (12), 1749–1757.

(2) Marmottant, P.; van der Meer, S.; Emmer, M.; Versluis, M.; de Jong, N.; Hilgenfeldt, S.; Lohse, D. A Model for Large Amplitude Oscillations of Coated Bubbles Accounting for Buckling and Rupture. *J. Acoust. Soc. Am.* **2005**, *118* (6), 3499–3505. https://doi.org/10.1121/1.2109427.

(3) Duncan, P. B.; Needham, D. Test of the Epstein-Plesset Model for Gas Microparticle Dissolution in Aqueous Media: Effect of Surface Tension and Gas Undersaturation in Solution. *Langmuir ACS J. Surf. Colloids* **2004**, *20* (7), 2567–2578. https://doi.org/10.1021/la034930i.

(4) Kim, D. H.; Costello, M. J.; Duncan, P. B.; Needham, D. Mechanical Properties and Microstructure of Polycrystalline Phospholipid Monolayer Shells: Novel Solid Microparticles. *Langmuir* **2003**, *19* (20), 8455–8466. https://doi.org/10.1021/la034779c.

(5) Hoff, L. *Acoustic Characterization of Contrast Agents for Medical Ultrasound Imaging*; Springer Science & Business Media, 2013.

(6) Lum, J. S.; Dove, J. D.; Murray, T. W.; Borden, M. A. Single Microbubble Measurements of Lipid Monolayer Viscoelastic Properties for Small Amplitude Oscillations. *Langmuir ACS J. Surf. Colloids* **2016**, *32* (37), 9410–9417. https://doi.org/10.1021/acs.langmuir.6b01882.